AGU PUBLICATIONS

JGR

Journal of Geophysical Research: Oceans

INTRODUCTION TO A SPECIAL SECTION

10.1002/2017JC012727

Special Section:
Oceanic Responses and Feedbacks to Tropical Cyclones

Key Points:
- Assimilation of AXBT observations has large impacts on reducing forecast errors in the COAMPS-TC prediction of ocean temperature
- The impact of adjoint-based targeted ocean observation are sensitive to the prestorm ocean conditions, TC-induced cold wake, and the TC model forecast track errors

Correspondence to:
S. Chen,
sue.chen@nrlmry.navy.mil

Citation:
Chen, S., J. A. Cummings, J. M. Schmidt, E. R. Sanabia, and S. R. Jayne (2017), Targeted ocean sampling guidance for tropical cyclones, *J. Geophys. Res. Oceans*, *122*, 3505–3518, doi:10.1002/2017JC012727.

Received 1 FEB 2017
Accepted 19 APR 2017
Accepted article online 25 APR 2017
Published online 13 MAY 2017

Targeted ocean sampling guidance for tropical cyclones

Sue Chen[1], James A. Cummings[2], Jerome M. Schmidt[1], Elizabeth R. Sanabia[3], and Steven R. Jayne[4]

[1]Naval Research Laboratory, Monterey, California, USA, [2]Science Applications International Corporation, Monterey, California, USA, [3]Oceanography Department, United States Naval Academy, Annapolis, Maryland, USA, [4]Woods Hole Oceanographic Institution, Woods Hole, Massachusetts, USA

Abstract A 3-D variational ocean data assimilation adjoint approach is used to examine the impact of ocean observations on coupled tropical cyclone (TC) model forecast error for three recent hurricanes: Isaac (2012), Hilda (2015), and Matthew (2016). In addition, this methodology is applied to develop an innovative ocean observation targeting tool validated using TC model simulations that assimilate ocean temperature observed by Airborne eXpendable Bathy Thermographs and Air-Launched Autonomous Micro-Observer floats. Comparison between the simulated targeted and real observation data assimilation impacts reveals a positive maximum mean linear correlation of 0.53 at 400–500 m, which implies some skill in the targeting application. Targeted ocean observation regions from these three hurricanes, however, show that the largest positive impacts in reducing the TC model forecast errors are sensitive to the initial prestorm ocean conditions such as the location and magnitude of preexisting ocean eddies, storm-induced ocean cold wake, and model track errors.

Plain Language Summary A 3D variational ocean data assimilation adjoint approach is used to examine the impact of ocean observations on coupled tropical cyclone (TC) model forecast error for three recent hurricanes: Isaac (2012), Hilda (2015), and Matthew (2016). Targeted ocean observation regions from these three hurricanes, show that the largest positive impacts in reducing the TC model forecast errors are sensitive to the initial pre-storm ocean conditions such as the location and magnitude of pre-existing ocean eddies, storm-induced ocean cold wake, and model track errors.

1. Introduction

It is well known that the ocean supplies the energy for tropical cyclone (TC) intensification. However, it is often difficult to observe the ocean condition underneath a TC. Historically, in situ sampling of the upper-ocean during active TCs has been relegated to infrequent specialized TC field campaigns such as The Coupled Boundary Layers Air-Sea Transfer (CBLAST) [see *Black et al.*, 2007] and Impact of Typhoons on the Ocean in the Pacific (ITOP) [see *D'Asaro et al.*, 2014] that were sponsored by the Office of Naval Research. Recently, there are increasing efforts to routinely sample the TC inner core ocean structure over the Gulf of Mexico, Atlantic, and Eastern Pacific [*Sanabia et al.*, 2013; *Jaimes and Shey*, 2015]. In particular, the *Sanabia et al.* [2013] study showed there is a positive impact of the ocean heat content (OHC) derived from AXBT's on improvements of the Statistical Hurricane Intensity Prediction Scheme (SHIPS) [*DeMaria et al.*, 2005] and an atmosphere-ocean coupled TC prediction model [*Doyle et al.*, 2012]. The ocean background states, such as the sea surface temperature, OHC, stability [*Schade and Emanuel*, 1999; *Lloyd and Vecchi*, 2011], mixed layer depth [*Lin et al.*, 2008], salinity [*Jacob and Koblinsky*, 2007; *Blaguru et al.*, 2012], and mesoscale warm/cold ocean eddies [*Wu et al.*, 2007; *Jaimes et al.*, 2011; *Yablonsky and Ginis*, 2013; *Ma et al.*, 2013] are known ocean pathways to impact the TC intensity. The variability of the coastal ocean conditions is another critical aspect influencing the TC intensity changes during landfall which can cause large societal and economic impacts depending on whether the land falling storm rapidly intensifies or weakens as it approaches the coast.

To date, global observations of densely covered sea surface temperature (SST) made by infrared and microwave satellites are unable to provide reliable SST retrievals near the TC center due to cloud cover, rain, and sea state contamination [*Gentemann et al.*, 2010]. Therefore, routinely deployed in situ ocean instruments

that observe the vertical profile of ocean temperature, salinity, and currents near the storm are important additions to an effective measurement strategy. Such measurements can provide an improved representation of the ocean conditions in the path ahead of a moving TC, and improved initialization of both coupled and uncoupled TC models. However, obstacles remain as these in situ observations are often costly to obtain. Additional problems arise due to the uncertainty regarding the specific ocean parameters to collect, the type of ocean instruments to use, when and where to deploy these instruments, and the spatial and temporal sampling resolution required in order to obtain the largest impacts on improving the TC model forecast. The TC-ocean observing strategy is especially critical if the observational deployment resources are limited. Hence, it is highly desirable to know the optimal sampling strategy for a given TC impacted ocean region a few days ahead of time in order that the largest TC model improvements can be realized.

Up-to-date advanced techniques used to examine the optimal ocean sampling strategy from the literature include the use of adjoint and ocean Observing System Simulation Experiment (OSSE) methods [*Gelaro and Zhu*, 2009; *Halliwell et al*., 2015]. Recently, *Cummings and Smedstad* [2014] showed that an adjoint-based procedure based on a three-dimensional variational analysis is another accurate method to assess the impact of ocean observations. The advantage of using the analysis adjoint is that the data impact is solely due to assimilation of the observations at each update cycle time and not from the effect of air-sea coupling. To answer the question of where best to obtain the TC ocean observations that will positively benefit a given air-sea coupled TC model forecast, we examine the feasibility of applying a modified targeted observing form of the adjoint-based ocean data method used by *Cummings and Smedstad* [2014]. The data impact and newly developed targeted observing systems are applied to forecasts generated by the state-of-the-art Coupled Ocean/Atmosphere Mesoscale Prediction System for Tropical Cyclones (COAMPS-TC). Section 2 describes the targeting technique, the COAMPS-TC model, the experimental setup, and the verification methodology. Section 3 contains results from the assimilation of Airborne eXpendable BathyThermographs (AXBTs) and Air-Launched Autonomous Micro-Observer (ALAMO) floats. Verification of targeted ocean observation using the assimilation of these two in situ observations is provided in section 4. We give our summary and conclusions in section 5.

2. Methodology

2.1. Targeted Ocean Sampling

The adjoint targeting technique is based on the Navy Coupled Ocean Data Assimilation (NCODA) adjoint [*Cummings and Smedstad*, 2014]. The adjoint of a data assimilation system is used to calculate the sensitivity of model forecast error at the observation locations used in the analysis. This extension of the adjoint sensitivity method into observational space can provide estimates of the impacts of real data assimilation on reducing model forecast error [*Langland and Baker*, 2004a], as well as the impacts of synthetic observations for targeted observing [*Langland and Baker*, 2004b; *Langland and Baker*, 2007]. The procedures for calculating the impacts of observations on forecast error and for targeted observing are similar, but differ in two important ways. In both applications data impact (δe_{24}) is measured as the inner product of a 3-D adjoint sensitivity vector at the observation location J ($\partial J/\partial y$; output from the NCODA adjoint) and model-observation difference ($|y - x_b|$) expressed by the following data impact equation derived by *Langland and Baker* [2004a]

$$\delta e_{24} = \langle |(y - Hx_b)|, \partial J/\partial y \rangle \tag{1}$$

where J is the forecast error sensitivity, y is the observation, H is the forward operator, and x_b is the model first guess field. For the forecast error problem, the adjoint sensitivity vector is computed from the gradient of the difference between COAMPS-TC 24 and 36 h forecasts valid at the same time relative to a verifying analysis:

$$\Delta e_{24}^{36} = \langle (x_{24} - x_0) \cdot (x_{24} - x_0) \rangle - \langle (x_{36} - x_0) \cdot (x_{36} - x_0) \rangle \tag{2}$$

where x_{24} and x_{36} are the forecast states at 24 and 36 h length, and x_0 is the verifying analysis. The outer brackets represent a scalar inner product. The forecast error gradients are projected from model space to observation space using the adjoint of the NCODA variational assimilation procedure according to:

$$\partial J/\partial y = K^T \Delta e_{24}^{36} \tag{3}$$

where K^T is the adjoint of the Kalman gain matrix $K^T = [HBH^T + R]^{-1}HB$, with B and R the background and observation error covariance. The observation sensitivity vector $\partial J/\partial y$ is the forecast error gradient in

observation space; its elements exist at the observation locations. Equation (2) is a true measure of forecast error. In addition, the model-data differences used in the data impact equation (1) is the innovation vector, which is based on real observations.

For the targeted observing application, observation sensitivity is calculated for a future time when a verifying analysis is not available. As such, a proxy for the true forecast error must be used. Here we define the adjoint sensitivity vector for targeted observing simply as the squared difference between two ocean temperature forecasts of varying lengths (24 and 36 h) valid at the same time. Another constraint is that actual innovation values are not known for any of the observations that will be obtained at the targeting time. It is necessary, therefore, to generate pseudo observations (hereafter referred to as synthetic observations) defined as the difference between the analyzed state and the 24 h model forecast issued from that analysis. The synthetic targeted observations are generated at select forecast model locations in a prescribed pattern around the 24 h forecast position of the TC and model levels above 700 m in order to be consistent with maximum AXBT sampling depth. In the case of targeted observing, it is also not known if a positive impact (reduction in forecast error) corresponds with an increase or a decrease in the value of the proxy forecast error sensitivity vector. When calculating impacts in the targeting application the observation sensitivity and the synthetic innovations are specified using absolute values. In this way both the forecast error sensitivity and the synthetic observations contribute to a positive targeted impact value. The impact of a targeted observation then is a measure of a change in variance or magnitude of the forecast error cost function (difference between forecasts valid at the same time). A large change in variance is assumed to represent a large data impact and the potential for a reduction in the forecast error at the targeting time.

2.2. COAMPS-TC Model Setup

For TC forecasts presented here, we set the two inner-most COAMPS-TC atmospheric nests so that they cover an area of $\sim$1500 $\times$ 1500 km each. The horizontal grid spacing of the two inner nests is 15 and 5 km, respectively. These atmosphere nests are set to automatically follow the model forecast TC center, while the 45 km outermost coarse atmosphere domain within which they are embedded is set to an area that covers most of the whole ocean basin. The outermost grid remains in a fixed position throughout the entire forecast period. The atmospheric model component is cold started every 12 h using the National Oceanic and Atmospheric Administration (NOAA) Global Forecasting System (GFS) initial and boundary conditions. After this procedure, a TC vortex bogusing algorithm is used to remove the global model TC circulation and insert a Rankine vortex based on the warning message from the Joint Typhoon Warning Center and National Hurricane Center. After the initial TC bogusing, the model mass field is adjusted to the wind field [*Doyle et al*., 2012].

The ocean model component of COAMPS-TC is the Navy Coastal Ocean Model (NCOM) [*Martin*, 2000]. This model uses a hybrid vertical sigma-Z vertical coordinate with a very thin 0.5 m top ocean layer to provide a better prediction of the diurnal SST cycle. The NCOM turbulent mixing is handled using the parameterized Mellor Yamada level 2 scheme. The model's data assimilation cycle is every 12 h using NCODA. The initial and boundary conditions for NCOM are derived from either the global HYbrid Coordinate Ocean Model (HYCOM) or the global NCOM. The coupling interval between the COAMPS-TC atmospheric and ocean components is set to 10 min. The atmospheric model provides six forcing fields to the ocean and the ocean model feedbacks the SST using the Earth System Modeling Framework [*Chen et al*., 2010].

2.3. Verification Method

To validate the goodness of fit of the target sampling we compare the sea temperature targeted and impact maps from twin experiments. To obtain the targeted map, we generate synthetic profiles from the model runs that deny the AXBT and ALAMO observations but which otherwise assimilate the other ocean observation data types (see Table 1 in *Cummings and Smedstad* [2014]). The forecast error sensitivity is computed in the NCODA adjoint to determine impacts of the targeted AXBT and ALAMO deployments in the vicinity of 24 h forecasts of the tropical TC sea temperature. The synthetic AXBTs are sampled every 20 km in all directions out to a radius of $\sim$150 km from the storm center. This yields a total of 240 synthetic profiles in rectangular sampling patterns centered on the 24 h COAMPS-TC forecast position of hurricane. To display the impact, the synthetic AXBT locations are color coded by the magnitude of the expected profile data

Table 1. Number of AXBT and ALAMO Profiles That Are Assimilated in NCODA

Tropical Cyclone	Isaac	Hilda	Matthew
AXBT	57	36	35
ALAMO	0	20	7

impact. Profile data impacts are calculated as the sum of the impacts at each profile level normalized by the number of profile levels.

The second forecast experiment assimilated observed 1 m high-vertical resolution AXBTs and ALAMO temperature profiles. Again, we use the NCODA adjoint to compute the sea temperature impact maps. The spatial correlation between the assimilated observation impact and the targeted maps gives a measurement of the accuracy of the targeted ocean observations. Negative values of data impacts indicate locations where assimilation of AXBT and ALAMO profile observations reduced 24 h forecast error of ocean temperature in COAMPS-TC. Data impacts are calculated for all levels in each profile. Impacts are normalized by the number of levels in a profile so that impacts from a variety of ocean data types, such as single level SST observations and Argo profiling floats, can be compared.

Additionally, we objectively assess the targeted ocean sampling skill by computing the linear correlation of the assimilation and targeted impact factors at targeted points and the actual AXBT and ALAMO observations that are within 50 km distance of each other. This distance is within the range of typical COAMPS-TC 36 h track error (∼50 nautical miles). The actual AXBT and ALAMO observations will never be exactly coincident with the targeted locations due to model track errors. The near collocated impact factors then are summed in specified depth interval ranges, i.e., 0–20, 20–50, 50–100, 100–200, 200–300, 300–400, and 400–500 m.

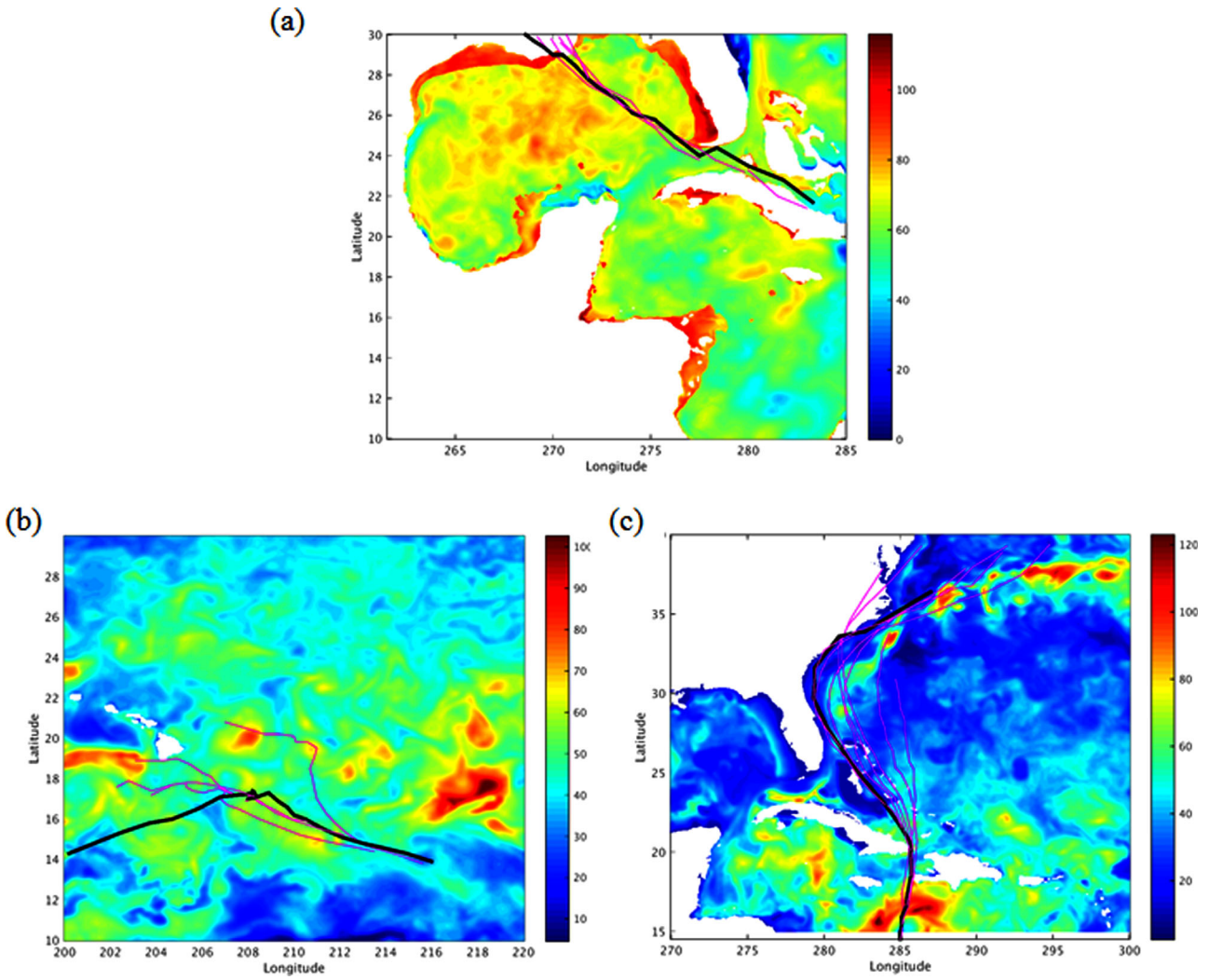

Figure 1. NCODA analyzed OHC (kJ m^{-2}) for: (a) Hurricane Isaac on 1200 UTC 26 August 2012, (b) Hurricane Hilda on 1200 UTC 9 August 2015, and (c) Hurricane Matthew on 1200 UTC 3 October 2016. The solid lines represent the observed (black) and COAMPS-TC 5 day forecast (magenta) tracks.

Table 2. Description of COAMPS-TC Experiments

Experiments	Isaac	Hilda	Matthew
Simulation Periods	25–29 August 2012	10–14 August 2015	3–9 October 2016
Assimilation	Atmos:12 × 4 km	Atmos: 45 × 15 × 5 km	Atmos: 45 × 15 × 5 km
	Ocean: 4 km	Ocean: 5 km	Ocean: 5 km
	With AXBT	With AXBT and ALAMO	With AXBT and ALAMO
Targeted	Atmos:12 × 4 km	Atmos: 45 × 15 × 5 km	Atmos: 45 × 15 × 5 km
	Ocean: 4 km	Ocean: 5 km	Ocean: 5 km
	Without AXBT	Without AXBT and ALAMO	Without AXBT and ALAMO

2.4. Experimental Design

To illustrate the usefulness of the adjoint-based targeted ocean sampling tool, we select three recent TC cases (Isaac, Hilda, and Matthew) that occurred in the Gulf of Mexico (GOM), Eastern Pacific (EPAC), and Atlantic (ATL) ocean basins, respectively. These three hurricanes all had the special AXBT and/or ALAMO floats deployed by the United States Naval Academy (USNA). Hurricane Isaac [*Berg*, 2013; *Jaimes and Shay*, 2015] entered the GOM on 24 August 2012 before making landfall twice on 30 August in southern Louisiana as Saffir-Simpson hurricane category (hereafter referred to as CAT) one wind scale. The movement of the Isaac eye back to the ocean after the first landfall was due to blocking induced by a midlevel atmosphere ridge located to the northwest of Isaac. Special AXBT observations were deployed during 22–30 August, 2012 following the Isaac track.

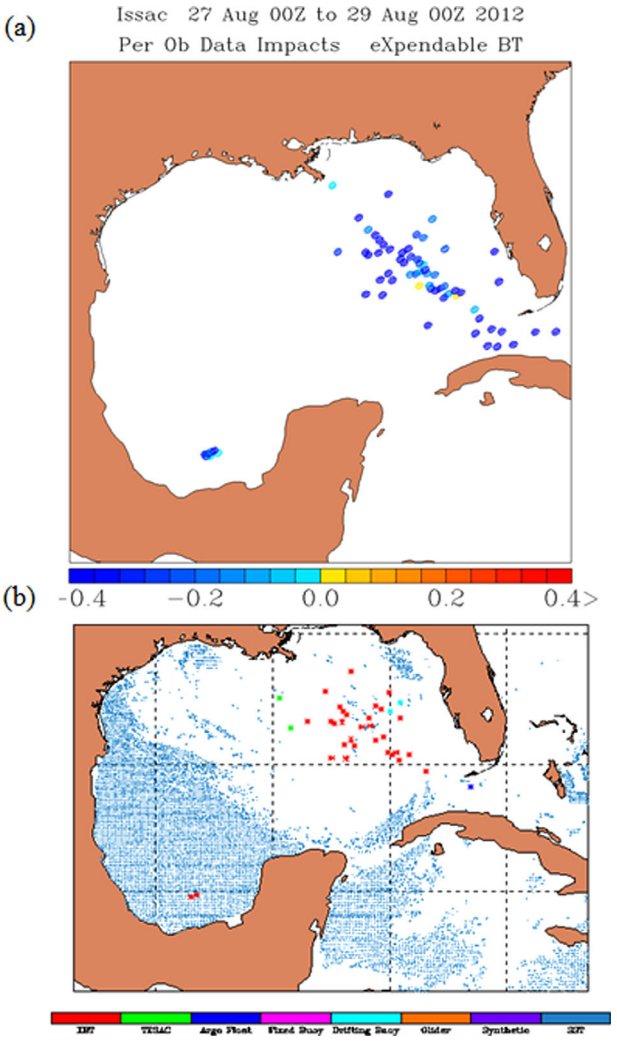

Figure 2. Hurricane Isaac (b) AXBT perobservation impact for the period of 27–29 August 2012. Negative values (cool colors) indicate that assimilation of the profile reduced COAMPS-TC 24 h sea tempertaure forecast error. Positive values (warm colors) indicate that assimilation of the profile increased the 24 h forecast error. (b) Composite map of different types of sea temperature observations used in NCODA analysis for (a) Hurricane Isaac on 1200 UTC 28 August 2011.

Hurricane Hilda [*Blake and Jelsema*, 2016] was a long-lived storm that initiated over the Eastern Pacific. This storm transversed northwestward and was eventually downgraded to a tropical depression over the central Pacific. Hilda reached CAT 4 hurricane strength on 8 August, during which time the USNA was able to deploy both AXBT and ALAMO for consecutive days through 12 August 2015.

Hurricane Matthew (2016) was a late-season hurricane that caused widespread severe flooding in Florida and the South and North Carolina coasts that resulted in 44 deaths in the US. Hurricane Matthew was the first Atlantic CAT 5 hurricane to strike the U.S. since 2007. The USNA deployed both the AXBT and ALAMO off the east coast of Florida after Hurricane Matthew made an unusual northwestward shift in track after devastating Haiti. Compared with the denial experiments, assimilation of the AXBT and ALAMO data for Hurricane Hilda and Matthew improves the track forecast for all lead times. While the improvement of intensity forecast for Hurricane Hilda and Matthew only lasts 24 h, the mean improvements

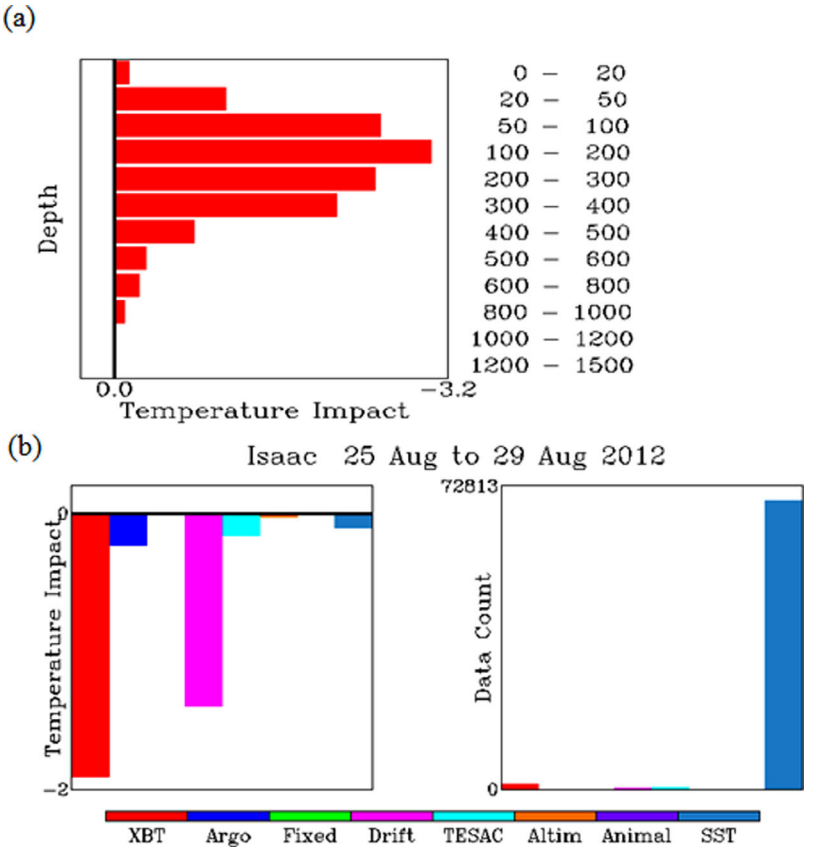

Figure 3. (a) A composite of perobservation AXBT vertical impactsduring the period of 25–29 August 2012 for Hurricane Isaac. (b) Hurricane Issac sea surface temperature observation impact normalized by the number of samples from AXBT, ARGO profiler, fixed buoys, drifting buoys with thermisor chains, gliders (TESAC), synthetic profiles derived from saltellite altimter SSH, and various sources of SST (satellite and in situ).

for the track and intensity forecasts are 21 nm and 13.6 m/s, respectively. However, because of the relative small sample size, the track and intensity presented here are not statistically significant.

Figure 1 shows the corresponding observed and COAMPS-TC forecast tracks for these three Hurricanes. The number of AXBT and ALAMO floats that are assimilated by NCODA into COAMPS-TC is listed in Table 1. A series of COAMPS-TC simulations with and without the AXBT and ALAMO assimilations (hereafter is referred to as the assimilation and deny twin experiments) are performed to assess the TC sea temperature forecast impacts from these special in situ ocean observations. For the Hurricane Isaac experiment, the COAMPS-TC domain configuration includes 60 vertical levels of two atmospheric domains (grid spacing of 12 and 4 km, respectively). The 4 km nest was set to automatically follow the TC center. The horizontal grid resolution of the ocean domain was set to 4 km with 50 vertical levels and 20 Z-levels in the upper ocean. The model was cold started from 0000 UTC, 25 August 2012. The NCOM initial and boundary conditions are from the global NCOM forecasts. The assimilation covers the period from 25 to 29 August 2012 with each forecast length set to 5 days. The model configuration for the Hilda and Matthew experiments is similar to the Hurricane Isaac experiments except the inner most atmosphere nest is set to 5 km and the ocean is also run at 5 km. The atmosphere model in each of these experiments was set to 40 vertical levels. The assimilation periods for Hurricane Hilda and Hurricane Matthew are from 10 to 14 August 2015 and 3 to 9 October 2016, respectively. Table 2 lists these COAMPS-TC experiments.

3. AXBT and ALAMO Assimilation Impacts

3.1. Hurricane Isaac

The ocean conditions before the passage of Hurricane Isaac in GOM was dominated by a large warm core eddy (WCE) that was centered in the GOM. It was shielded from the Gulf loop-current that was present

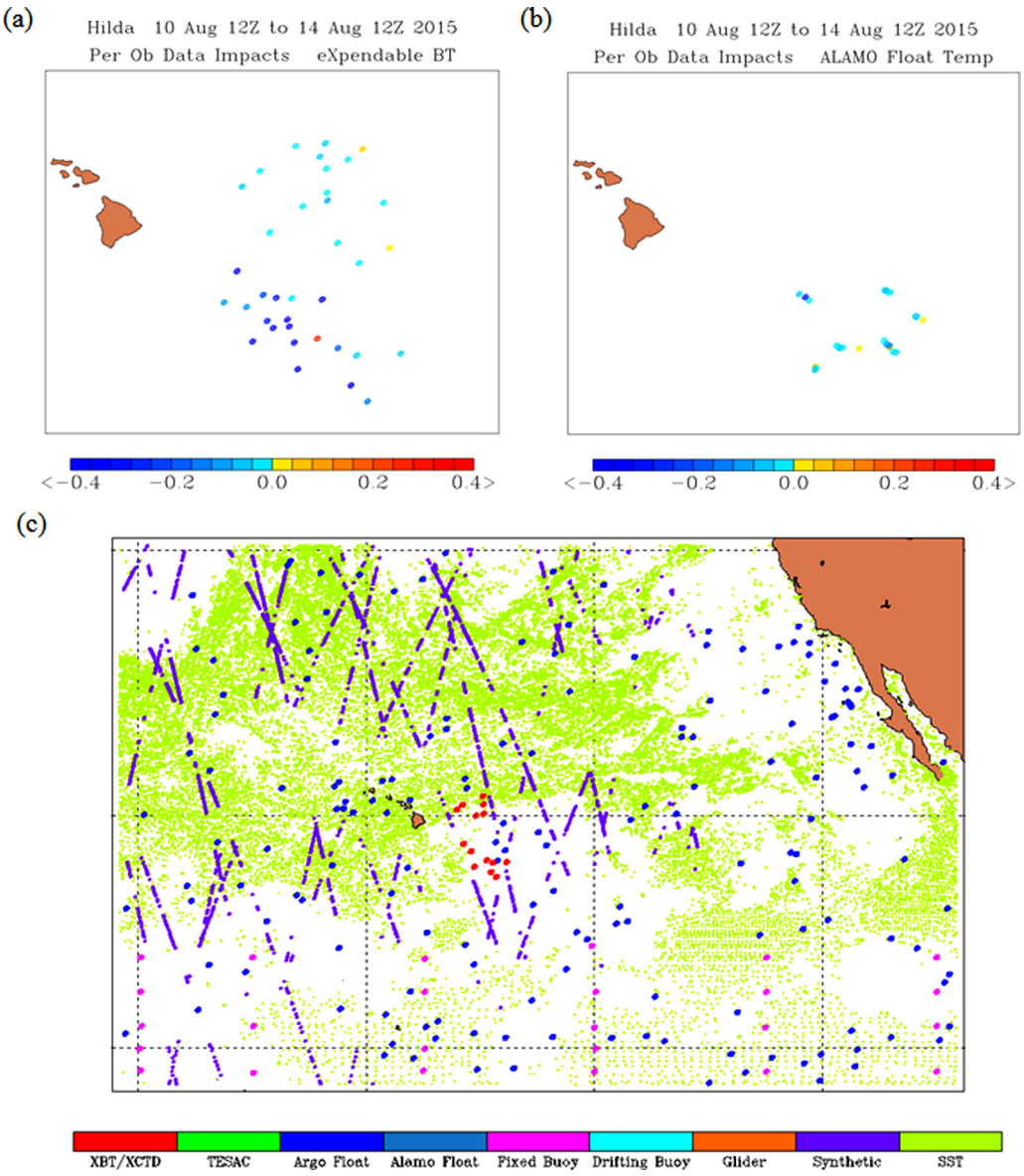

Figure 4. As in Figure 2 but for Hurricane Hilda (a) AXBT and (b) ALAMO impacts during 10–14 August 2015. (c) Composite map of different types of sea temperature observations used in NCODA analysis on 1200 UTC 10 August, 2015.

earlier in the spring with no cold water intrusion of the loop-current occurring during the passage of Isaac [*Jaimes and Shay*, 2015]. The sea gridded sea surface height anomaly (SSHA) product from Colorado Center for Astrodynamics Research (CCAR) indicates there was a pair of smaller cold core eddies (CCE) located on the eastern flank of this WCE. Compared to CCAR SSHA, the WCE and CCEs magnitude, size, and position in COAMPS-TC initial condition have a bias (not shown). The position and magnitude errors of these oceanic eddies are corrected by the assimilation of the AXBT observations.

The analysis adjoint data impact map shows the impact of assimilation of AXBT observations on COAMPS-TC sea temperature forecast errors (Figure 2). Negative values indicate a forecast error reduction while positive values indicate that assimilation of the AXBT profile actually increased model forecast error. It can be seen that all but two of the AXBTs assimilated between 25 and 29 August reduced COAMPS-TC forecast sea temperature errors. The horizontal distribution of the AXBT ocean temperature impacts shows that assimilation of the AXBT consistently reduced sea temperature forecast errors throughout the life cycle of the storm. A large portion of the error reduction was likely derived from reducing the errors in the innovation vector

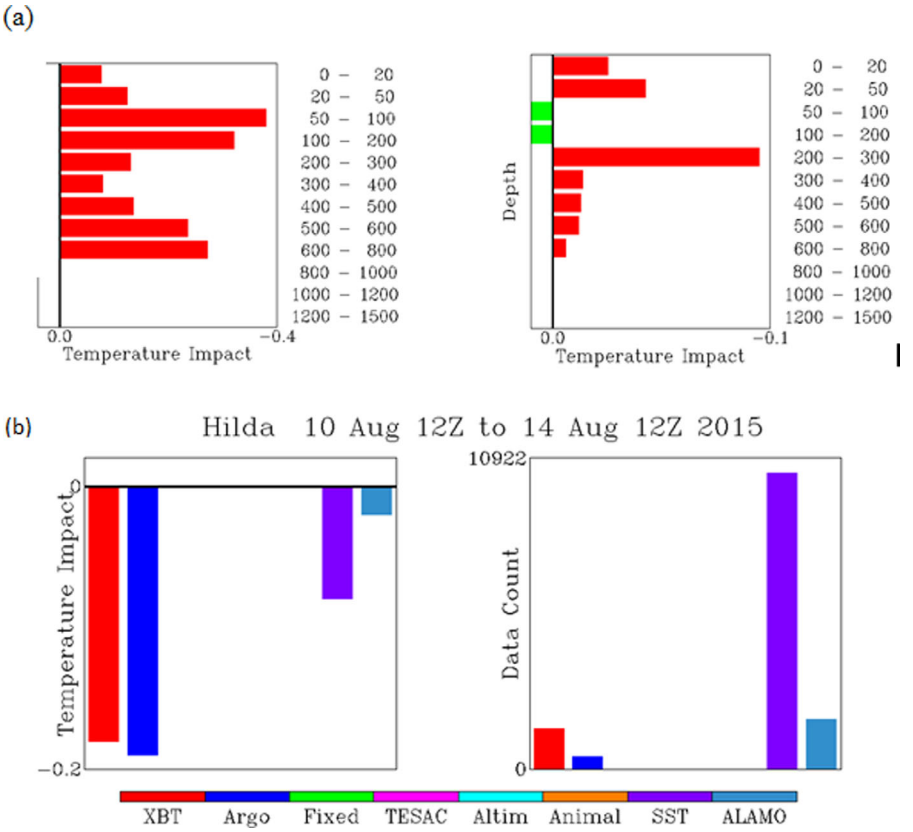

Figure 5. (a) A composite perobservation (left) AXBT and (right) ALAMO vertical impact during the period of 10-14 August 2015 for Hurricane Hilda. (b) Hurricane Hilda sea surface temperature observation impact normalized by the number of samples from AXBT, ARGO profiler, fixed buoys, gliders (TESAC), altimeters, various sources of SST (satellite and in situ), and ALAMO.

(correcting the model first guess forecast field) from repeated insertion of new AXBT profiles into the system. Figure 3a shows that the forecast temperature error reduction from assimilation of AXBT extended across all AXBT sampling depths with the lagest error reduction occuring in the 100–200 m depth range, which is approximately the depth of the permannent thermocline in the Gulf of Mexico. Further, compared to other observation types assimilated, the AXBT has the largest perobservation impact, when normalized by the number of observations, in reducing the model forecast sea temperature error (Figure 3b).

3.2. Hurricane Hilda

For COAMPS-TC Hurricane Hilda simulations, squared temperature differences between 24 and 36 h forecasts valid at the same time relative to verifying analyses during the 10–14 August 2015 time period shows that this measure of forecast error varies with location and depth (not shown). Relatively large ocean temperature forecast errors at the surface clearly reflect the hurricane circulation in the atmosphere. Below the surface, the ocean forecast errors are associated more with the storm center and tend to diminish in magnitude with depth. These sea temperature forecast errors evolve with time as the storm intensifies and weakens. The composite AXBT and ALAMO assimilation impact maps for this period reveal that assimilation of three AXBT and two ALAMO temperature profiles increased COAMPS-TC forecast sea temperature errors, while assimilation of all remaining AXBT and ALAMO profiles reduced forecast error during the observing period (Figure 4). Figure 5a shows that assimilation of AXBT profiles reduced ocean temperature forecast error at all observing depths, with maximum impacts in the 50–100 depth range. However, assimilation of sea temperature data from the ALAMO floats was found to increase COAMPS-TC ocean temperature forecast errors between 50 and 200 m when impacts are averaged across all ALAMO floats. This result likely indicates assimilation of erroneous observations that contained very large model-data innovations, which is being investigated with the ALAMO float provider. Comparison of impacts of assimilation of AXBT and ALAMO profile floats with other ocean observing systems assimilated is shown in Figure 5b. It was found

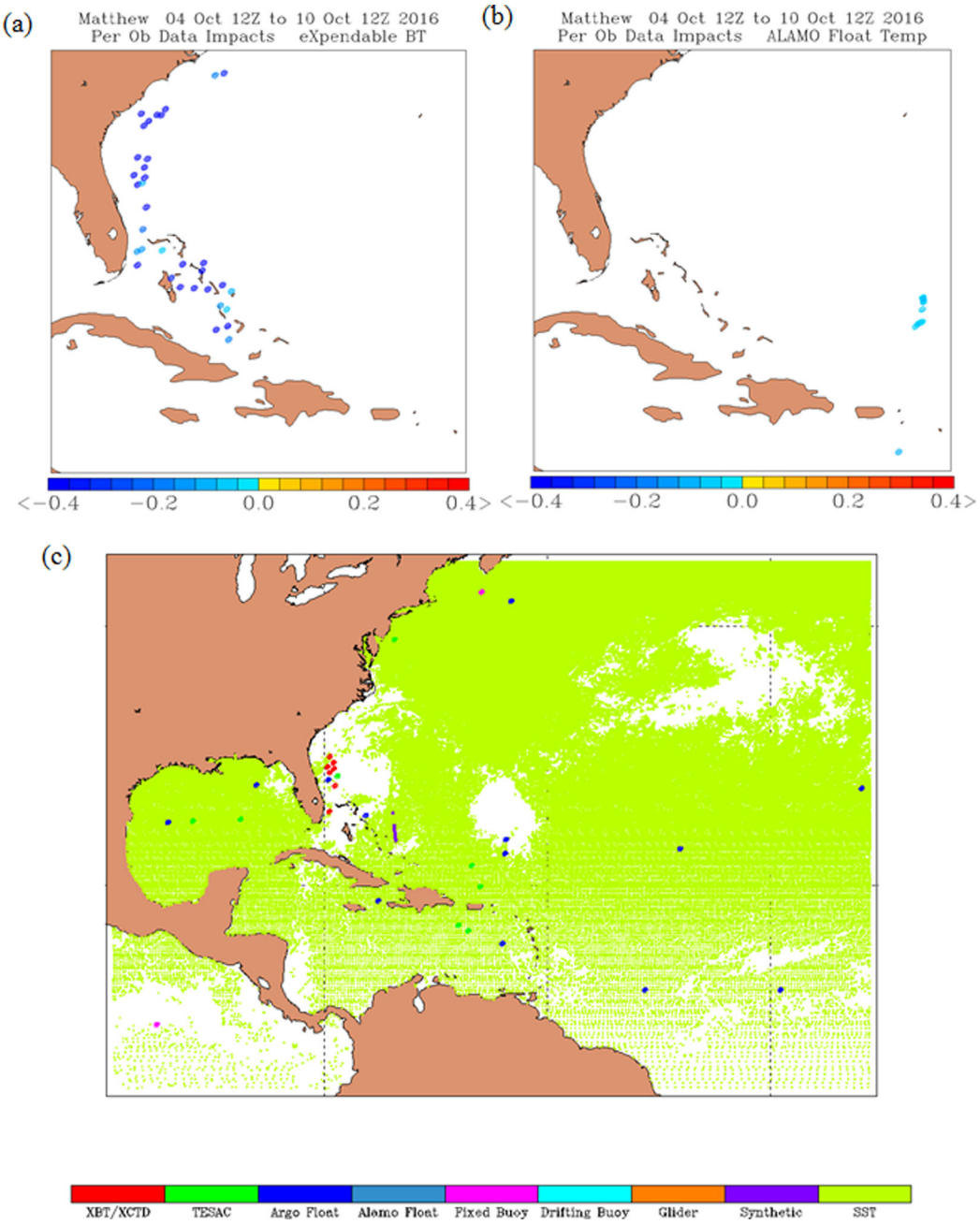

Figure 6. (a and b) As in Figure 4, but for Hurricane Matthew during 4–10 October 2016. (c) Composite map of different types of sea temperature observations used in NCODA analysis on 1200 UTC 7 October 2016.

that assimilation of Argo floats has the greatest impact on reducing ocean temperature forecast error with assimilation of AXBT a close second. Assimilation of the various sources of SST was third, while assimilation of ALAMO floats was fourth. These impact rankings indicate that assimilation of observing systems that routinely sample large geographic areas, such as Argo and SST, tend to have greater data impacts. The high rank of assimilating AXBT observations, however, indicates that improved observing of specific events such as the passage of hurricanes is also beneficial at reducing COAMPS-TC ocean temperature forecast error. ALAMO floats are essentially Argo equivalents. As indicated above, it is believed that some data issues with the ALAMO temperature data between 50 and 200 m depth degraded the overall impact of the ALAMO data.

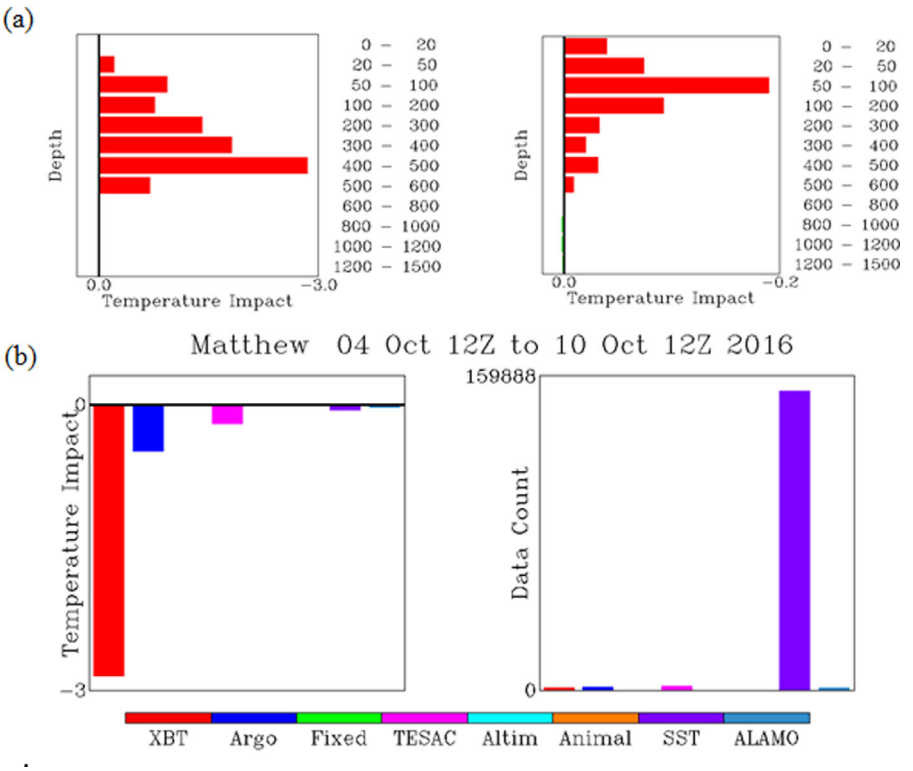

Figure 7. As in Figure 5, but for Hurricane Matthew during the period of 4–10 October 2016.

3.3. Hurricane Matthew

Both the AXBT and ALAMO floats are also available for the Hurricane Matthew assimilation. Figure 6 shows the geographic distribution of the impacts of assimilating AXBT and ALAMO. The AXBT locations follow the path of the storm, but the ALAMO floats were deployed earlier in the season and are located east of Haiti. The impact maps for Matthew show that assimilation of all AXBT and ALAMO floats reduced COAMPS-TC sea temperature forecast error. However, in contrast to the Hurricane Isaac and Hilda cases where the largest AXBT subsurface impacts are at the base of the mixed layer and thermocline, the AXBT influence on Hurricane Matthew has the largest impact on reducing COAMPS-TC subsurface sea temperature forecast errors at a depth of 400–500 m (Figure 6a). The maximum impact of ALAMO is shallower at a depth of 50–100 m, but recall that the geographic locations of AXBT and ALAMO data do not coincide in the Hurricane Mathew case. When comparing ocean observing systems, we found assimilation of the AXBT observations is the single most important observing system that reduced COAMPS-TC forecast errors (Figure 7).

4. Optimal Targeted Ocean Sampling

The targeted impact maps are created using the COAMPS-TC forecast profiles from the data denial experiments (Table 2). The results show the targeted impact patterns varies with time and the given storm system. The targeted impact pattern for Hurricane Isaac suggests observations near the storm center and along the two front quadrants will reduce future COAMPS-TC NCOM ocean model forecast errors (Figure 8a). The largest impact on the subsurface sea temperature forecasts extends from the sea surface down to 100 m (Figure 8b). Recall that in section 3.1, the model had position and magnitude errors for a pair of GOM warm and cold eddies that were located to the left and right of Hurricane Isaac track, respectively.

In contrast to the Hurricane Isaac case, the targeted impact patterns for Hurricane Hilda and the Hurricane Matthew cases suggest that observations taken near the storm center and along the storm track to the southeast in the cold wake region will reduce future ocean model forecast errors (Figures 9a and 10a, respectively). Note that the COAMPS-TC forecast tracks indicate that the storms are moving to the

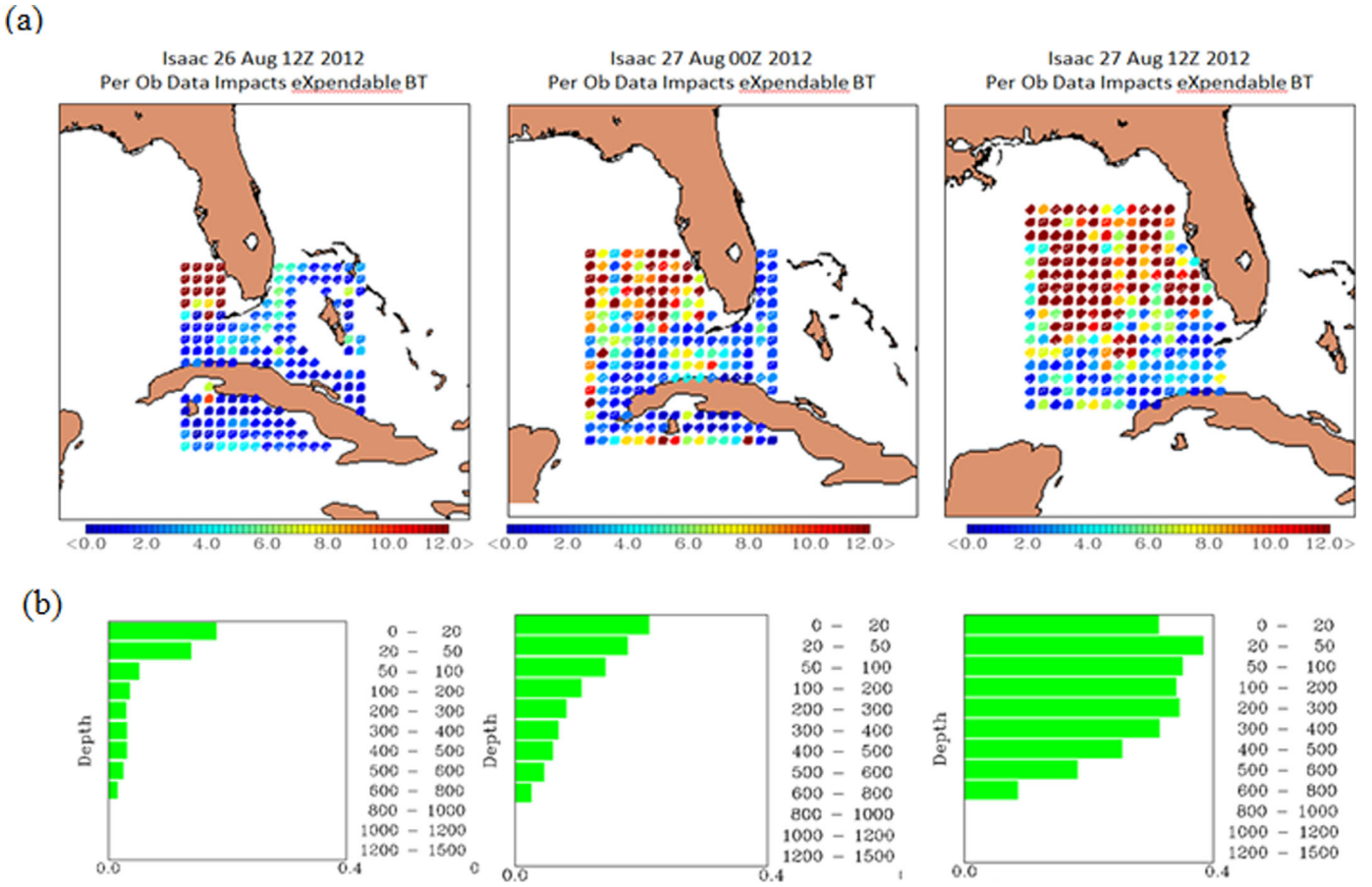

Figure 8. Plots showing the expected targeted total impacts of ocean sea temperature for (a) spatially and, (b) as a function of depth in the sampling patterns generated in Figure 8a for Hurricane Isaac (2012) valid at 1200 UTC 26 August, and 0000 UTC and 1200 UTC 27 August 2011. Observation locations with warmer colors in Figure 8a represent the likelihood those ocean probes have larger impacts on reducing COAMPS-TC forecast sea temperature forecast errors.

northwest. The TC-induced trailing ocean cold wakes are then found to the right rear of the storm track. Figures 9b and 9c show the impact of the targeted profiles as a function of depth summed within the specified depth interval ranges. The targeted data impacts are greatest in the upper 100 m of the water column near the surface, with somewhat higher values in the two rear quadrants of the cold wake region and again in vicinity of the mixed layer depth, which was near 50 m.

Comparison of the targeted profiles within 50 km of the AXBT or ALAMO observations in seven sampling layers reveals that the maximum mean spatial linear correlation is ∼0.53 at the 400–500 m layer with minimum/maximum correlation of 0.11/0.93 for Hurricane Isaac, 0.16/0.43 for Hilda, and 0.35/0.79 for Matthew (see Table 3, 149 sample sizes). For Isaac, minimum correlations are at the surface with the highest correlations occurring in the 100–200 m depth layer. For Hilda, the minimum correlation is slightly deeper in the 20–50 m layer with the maximum correlation in the deepest layer at 400–500 m. For Matthew, the minimum correlation occurs at the greatest depth layer 400–500 m, with the maximum correlation in the 200–300 m layer. This variability is not surprising given the very different vertical ocean thermal structure that is present in the three ocean basins where the storms occurred. The magnitude of the correlation appears to be anti-correlated to the COAMPS-TC track errors. The correlation of the targeted impacts with the assimilation impacts is low in the COAMPS-TC runs that have larger track errors. The correlation for these seven depth layers shows, in general, that the correlation between the targeted and assimilation impacts are higher for subsurface than over the upper 20 m of the ocean layer. A plausible cause may be the near surface model errors are effectively constrained from assimilation of the more densely covered SST observations. Forecast error reduction of ocean temperature from assimilation of SST observations does not extend much beyond the mixed layer depth, whereas below that depth forecast error reduction occurs from assimilation of ocean

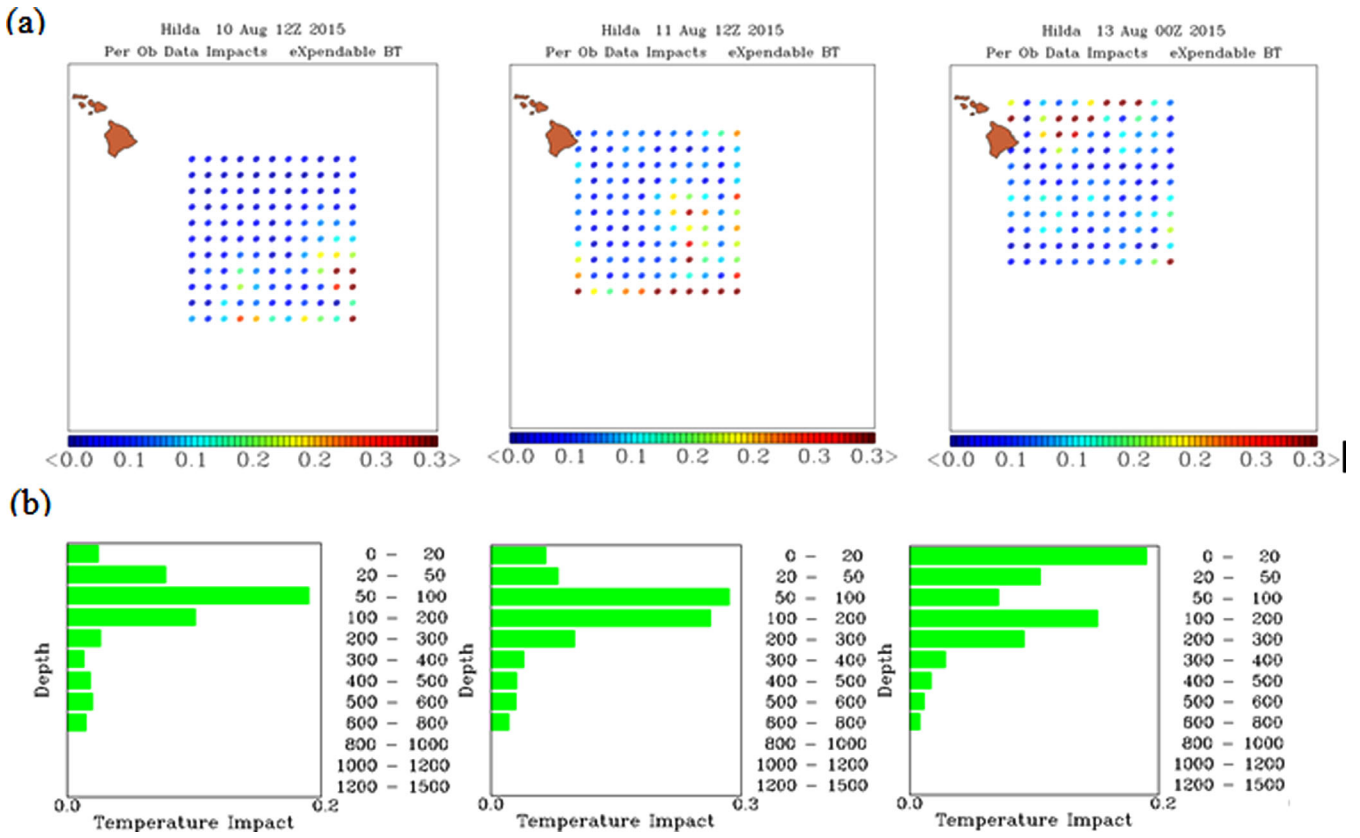

Figure 9. As in Figure 8, but for Hurricane Hilda valid at 1200 UTC 10 August 1200 UTC 11 August, and 0000 UTC 13 August 2015.

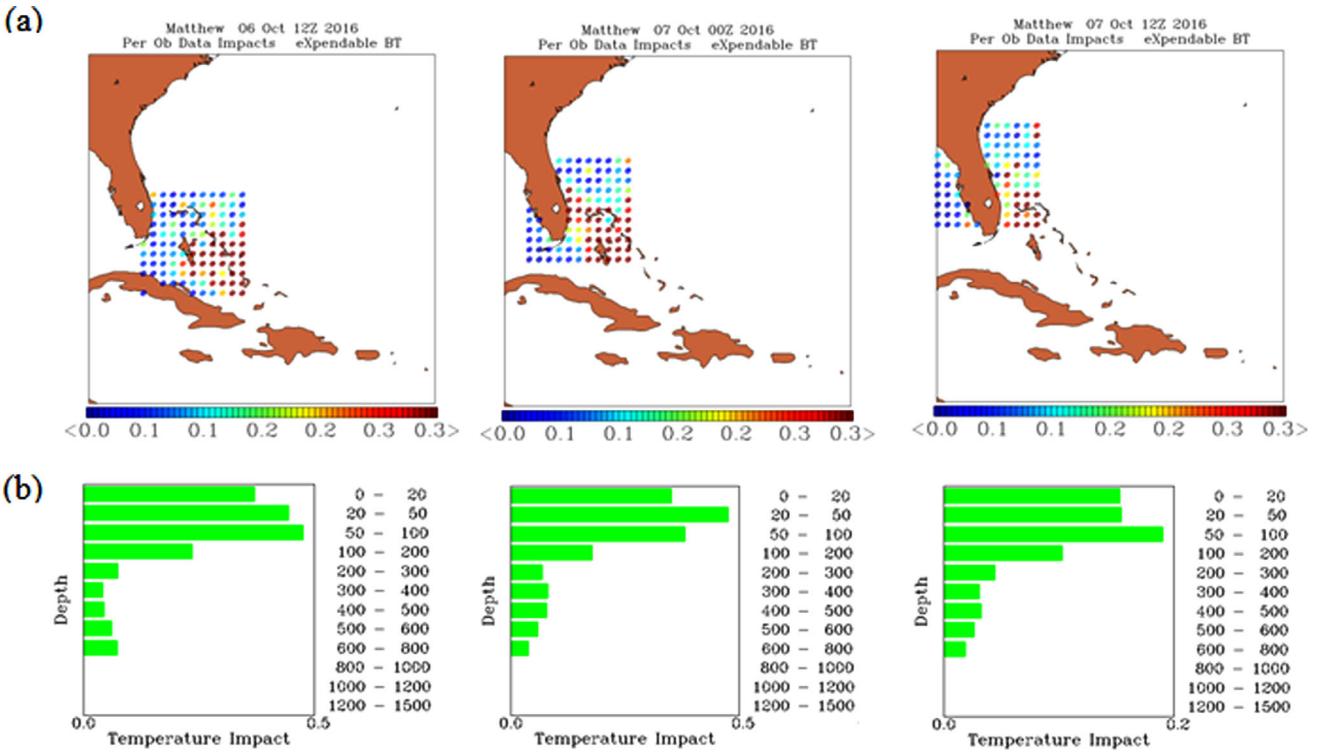

Figure 10. As in Figure 8, but for Hurricane Matthew valid at 1200 UTC 6 October, 0000 UTC 7 October, and 1200 UTC 7 October 2016.

Table 3. Spatial Correlation of the Assimilation and Targeted Impact Factors

Depth Layer	Total Mean	Isaac	Hilda	Matthew
0–20 m	0.28	0.11	0.16	0.53
20–50 m	0.35	0.11	0.15	0.59
50–100 m	0.36	0.54	0.25	0.55
100–200 m	0.41	0.93	0.24	0.56
200–300 m	0.44	0.84	0.20	0.79
300–400 m	0.38	0.82	0.21	0.63
400–500 m	0.53	0.88	0.43	0.35

profiles. Although the sample size studied here is limited, the optimal sampling results reflect the errors in the COAMPS-TC initial ocean background, especially the position and strength of preexisting eddies as well as COAMPS-TC track errors.

5. Summary and Conclusions

The targeted TC ocean sampling strategy is important in advancing the research in TC air-sea interaction. This is particularly the case for modeled forecasts of TC intensity changes that are critically influenced by the structure of the underlying ocean beneath the TC track. We examined the 24–36 h targeted and assimilated ocean temperature profiles generated from the coupled COAMPS-TC forecasts of three Hurricanes (Isaac, Hilda, and Matthew). Information on where to deploy the ocean observations that can yield the largest benefit to reduce subsequent COAMPS-TC forecast of ocean temperature errors 24–36 h ahead of the time is validated using experiments that assimilated special AXBT and ALAMO observations. The maximum mean linear correlation between the assimilation impact map and the targeted impact map is 0.53 at 400–500 m. There are notable differences in the patterns of the largest impact region for these three hurricanes. The AXBT and ALAMO assimilation impact maps show the sensitive area is in the center and two front quadrants of Hurricane Isaac. For Hurricanes Hilda and Matthew, the largest impacts are located in center and to the rear-right of the storm in a region of storm-induced cold ocean wake. For Hurricane Isaac, assimilation of the AXBT reduced the COAMPS-TC initial condition errors of the position and magnitude of GOM cold and warm eddies. Assimilation of the AXBT in the TC ocean cold wake regions of Hurricane Hilda and Matthew reduced the COAMPS-TC initial condition errors of the cold wake.

The results indicate that the skill of adjoint-based ocean targeting patterns is sensitive to the prestorm ocean conditions and the coupled TC model track errors. In addition, the generality of the adjoint method also allows the evaluation of assimilation impacts for multiple ocean sensors simultaneously in COAMPS-TC. For Hurricanes Isaac and Matthew, it was shown that AXBT observations have the largest perobservation impact than other types of assimilated ocean observing systems. In the Hilda case, the impact of assimilation of Argo was slightly greater than assimilation of AXBT. We demonstrated that a new innovative adjoint-based targeted ocean sampling technique is capable of providing skillful guidance on where to deploy the targeted ocean observations in order to reduce subsequent coupled TC model forecasts 24–36 h in advance. The coupled COAMPS-TC model is used here to demonstrate this methodology, but this technique could also be readily applicable to other ocean observations such as salinity and currents and other coupled TC models.

One important topic that has not been touched on here is the TC track, intensity, and structure improvements from targeted ocean observations. Future research using the coupled TC model to systematically examine a large sample of TC cases that can yield a statistically significant evaluation is warranted. Future advancements in coupled adjoint data assimilation technique will also provide a better quantification of the TC responses from targeted ocean observations.

Acknowledgments
The authors wish to thank COAMPS-TC development team and the sponsorship of Office of Naval Research and National Oceanic and Atmospheric Administration. Chen, Cummings, and Schmidt are supported by ONR grant N0001416WX01949. Sanabia is sponsored by ONR grants N0001416WX01384 and N0001416WX01262. Jayne is supported by NOAA grant NA13OAR4830233. Computational resources obtained from the Department of Defense High Performance Computing Modernization Program are greatly appreciated. The COAMPS model, high-resolution AXBT, and ALAMO data for Hurricanes Isaac, Hilda, and Matthew can be obtained by contacting the authors. Both the AXBT and ALAMO data were also transmitted in real time to the Global Telecommunication System (GTS).

References

Balaguru, K., P. Chang, R. Saravanan, L. R. Leung, Z. Xu, M. K. Li, and J. S. Hsieh (2012), Ocean barrier layers' effect on tropical cyclone intensification, *Proc. Natl. Acad. Sci. U. S. A.*, *109*, 14,343–14,347, doi:10.1073/pnas.1201364109.

Berg, R. J. (2013), Tropical cyclone report: Hurricane Isaac (AL092012), *Natl. Hurricane Cent. Tech. Rep.*, 78 pp., National Hurricane Center, Miami, Fla.

Black, P. G., et al. (2007), Airsea exchange in hurricanes: Synthesis of observations from the Coupled Boundary Layer AirSea Transfer experiment, *Bull. Am. Meteorol. Soc.*, *88*, 357–374, doi:10.1175/BAMS-88-3-357.

Blake, E. S., and J. Jelsema (2016), Tropical cyclone report: Hurricane Hilda (EP102015), *Natl. Hurricane Cent. Tech. Rep.*, 16 pp.

Chen, S., T. J. Campbell, H. Jin, S. Gabersek, R. M. Hodur, and P. Martin (2010), Effect of two-way air-sea coupling in high and low wind speed regimes, *Mon. Weather Rev.*, *138*, 3579–3602, doi:10.1175/2009MWR3119.1.

Cummings, J. A., and O. M. Smedstad (2014), Ocean data impacts in global HYCOM, *J. Atmos. Oceanic Technol.*, *31*, 1771–1791, doi:10.1175/JTECH-D-14-00011.1.

D'Asaro, E. A., et al. (2014), Impact of typhoons on the ocean in the Pacific, *Bull. Am. Meteorol. Soc.*, *95*, 1405–1418, doi:10.1175/BAMS-D-12-00104.1.

DeMaria, M., M. Mainelli, L. K. Shay, J. A. Knaff, and J. Kaplan (2005), Further improvements to the statistical hurricane intensity prediction scheme (SHIPS), *Weather Forecast.*, *20*(4), 531–543.

Doyle, J. D., et al. (2012), Real-time tropical cyclone prediction using COAMPS-TC, *Adv. Geosci.*, *28*, 15–28.

Gelaro, R., and Y. Q. Zhu (2009), Examination of observation impacts derived from observing system experiments (OSEs) and adjoint models, *Tellus, Ser. A*, *61*, 179–193, doi:10.1111/j.1600-0870.2008.00388.x.

Gentemann, C., F. J. Wentz, M. Brewer, K. Hilburn, and D. Smith (2010), Passive microwave remote sensing of the ocean: An overview, in *Oceanography From Space, Revisited*, edited by V. Barale, J. F. R. Gower, and L. Alberotanza, pp. 13–33, Springer, Heidelberg, Germany.

Halliwell, G. R., V. Kourafalou, M. Le Henaff, L. K. Shay, and R. Atlas (2015), OSSE impact analysis of airborne ocean surveys for improving upper-ocean dynamical and thermodynamical forecasts in the Gulf of Mexico, *Prog. Oceanogr.*, *130*, 32–46, doi:10.1016/j.pocean.2014.09.004.

Jacob, S. D., and C. J. Koblinsky (2007), Effects of precipitation on the upper-ocean response to a hurricane, *Mon. Weather Rev.*, *135*, 2207–2225, doi:10.1175/MWR3366.1.

Jaimes, B., and L. K. Shay (2015), Enhanced wind-driven downwelling flow in warm oceanic eddy features during the intensification of Tropical Cyclone Isaac (2012): Observations and theory, *J. Phys. Oceanogr.*, *45*, 1667–1689, doi:10.1175/JPO-D-14-0176.1.

James, B., L. K. Shay, and G. R. Halliwell (2011), The response of quasigeostrophic oceanic vortices to tropical cyclone forcing, *J. Phys. Oceanogr.*, *41*, 1965–1985, doi:10.1175/JPO-D-11-06.1.

Langland, R. H., and N. L. Baker (2004a), Estimation of observation impact using the NRL atmospheric variational data assimilation adjoint system, *Tellus, Ser. A*, *56*, 189–201, doi:10.1111/j.1600-0870.2004.00056.x.

Langland, R. H., and N. L. Baker (2004b), A technical description of the NAVDAS adjoint system, *NRL Tech. Memo. Rep. NRL/MR/7530-04-8746*, Marine Meteorology Division, Naval Research Laboratory, Montery, Calif.

Langland, R. H., and N. L. Baker (2007), Interpretations of an adjoint-derived observational impact measure—Reply, *Tellus, Ser. A*, *59*, 277–277, doi:10.1111/j.1600-0870.2006.00217.x.

Lin, I. I., C. C. Wu, I. F. Pun, and D. S. Ko (2008), Upper-ocean thermal structure and the western North Pacific category 5 typhoons: Part I: Ocean features and the category 5 typhoons' intensification, *Mon. Weather Rev.*, *136*, 3288–3306, doi:10.1175/2008MWR2277.1.

Lloyd, I. D., and G. A. Vecchi (2011), Observational evidence for oceanic controls on hurricane intensity, *J. Clim.*, *24*, 1138–1153, doi:10.1175/2010JCLI3763.1.

Ma, Z. H., J. F. Fei, L. Liu, X. G. Huang, and X. P. Cheng (2013), Effects of the cold core eddy on tropical cyclone intensity and structure under idealized air-sea interaction conditions, *Mon. Weather Rev.*, *141*, 1285–1303, doi:10.1175/MWR-D-12-00123.1.

Martin, P. J. (2000), Description of the Navy Coastal Ocean Model Version 1.0, *NRL Rep. 460 NRL/FR/7322/00/9962*, 45 pp., Oceanography Division, Naval Research Laboratory, Stennis, Miss.

Sanabia, E. R., B. S. Barrett, P. G. Black, S. Chen, and J. A. Cummings (2013), Real-time upper-ocean temperature observations from aircraft during operational hurricane reconnaissance missions: AXBT demonstration project year one results, *Weather Forecast.*, *28*, 1404–1422, doi:10.1175/WAF-D-12-00107.1.

Schade, L. R., and K. A. Emanuel (1999), The ocean's effect on the intensity of tropical cyclones: Results from a simple coupled atmosphere-ocean model, *J. Atmos. Sci.*, *56*, 642–651, doi:10.1175/1520-0469(1999)056<0642:TOSEOT>2.0.CO;2.

Wu, C. C., C. Y. Lee, and I. I. Lin (2007), The effect of the ocean eddy on tropical cyclone intensity, *J. Atmos. Sci.*, *64*, 3562–3578, doi:10.1175/JAS4051.1.

Yablonsky, R. M., and I. Ginis (2013), Impact of a warm ocean Eddy's circulation on hurricane-induced sea surface cooling with implications for hurricane intensity, *Mon. Weather Rev.*, *141*, 997–1021, doi:10.1175/MWR-D-12-002481.